Inorg. Chem. **2003**, *42*, 42–50

Fe(III) Coordination Properties of a New Saccharide-Based Exocyclic Trihydroxamate Analogue of Ferrichrome

Suraj Dhungana,[†] Susanne Heggemann,[‡] Peter Gebhardt,[‡] Ute Möllmann,[‡] and Alvin L. Crumbliss*[,†]

Department of Chemistry, Duke University, Box 90346 Durham, North Carolina 27708-0346, and Hans Knöll-Institut für Naturstoff-Forschung, Beutenbergstrasse 11a, D-07745 Jena, Germany

Received April 11, 2002

The coordination chemistry of a saccharide-based ferrichrome analogue, 1-*O*-methyl-2,3,4-tris-*O*-[4-(*N*-hydroxy-*N*-methylcarbamoyl)-*n*-butyrate]-α-D-glucopyranoside (H_3L), is reported, along with its pK_a values, Fe(III) and Fe(II) chelation constants, and aqueous-solution speciation as determined by spectrophotometric and potentiometric titration techniques. The use of a saccharide platform to synthesize a hexadentate trihydroxamic acid chelator provides some advantages over other approaches to ferrichrome models, including significant water solubility and hydrogen-bonding capability of the backbone that can potentially provide favorable receptor recognition and biological activity. The pK_a values for the hydroxamate moieties were found to be similar to those of other trihydroxamates. Proton-dependent Fe^{III}–H_3L and Fe^{II}–H_3L equilibrium constants were determined using a model involving the sequential protonation of the iron(III)– and iron(II)–ligand complexes. These results were used to calculate the formation constants, log $\beta_{110} = 31.86$ for $Fe^{III}L$ and 12.1 for $Fe^{II}L^-$. The calculated pFe value of 27.1 indicates that H_3L possesses an Fe(III) affinity comparable to or greater than those of ferrichrome and other ferrichrome analogues and is thermodynamically capable of removing Fe(III) from transferrin. $E_{1/2}$ for the $Fe^{III}L/Fe^{II}L^-$ couple was determined to be –436 mV from quasi-reversible cyclic voltammograms at pH = 9, and the pH-dependent $E_{1/2}$ profile was used to determine the $Fe^{II}L^-$ protonation constants.

Introduction

Iron is universally required for the growth of almost all living cells. Although iron is the most abundant transition metal in the biosphere, under aqueous-aerobic conditions and neutral pH, iron is present mostly as insoluble iron(III) hydroxide.[1] At pH = 7.4 and in the absence of chelating ligands, the total amount of soluble iron [$Fe^{3+}_{(aq)}$ + $Fe(OH)^{2+}_{(aq)}$ + $Fe(OH)_2{}^+_{(aq)}$] is as low as 10^{-10} M,[2] a concentration that is 4 orders of magnitude lower than the concentration required by microorganisms.[3] Microorganisms secrete siderophores, a class of highly specific Fe(III)-chelating agents, under iron-deficient conditions to sequester iron from the environment. These potent Fe(III)-specific chelators usually include either hydroxamate or catecholate functional groups for iron coordination, and their Fe(III)-chelating affinity largely determines the microbial bioavailability of iron.[4−9]

Siderophore-mediated iron acquisition from the environment involves solubilization (chelation) of Fe(III) from its highly insoluble hydroxide form, transport to and across the cell membrane, and deposition at an appropriate site within the cell.[4,5,8] Microbial siderophores exhibit high and specific affinity for Fe(III) (log $\beta > 30$)[4] for selective chelation of Fe(III) in the presence of other environmentally prevalent metal ions. The siderophore−iron complexes are recognized

* Address correspondence to this author. E-mail: alc@chem.duke.edu. Fax: (919) 660-1605.
† Duke University.
‡ Hans Knöll-Institut für Naturstoff-Forschung.

(1) Crichton, R. R. *Inorganic Biochemistry of Iron Metabolism: From Molecular Mechanism to Clinical Consequences*, 2nd ed.; Wiley: New York, 2001.
(2) Boukhalfa, H.; Crumbliss, A. L. *BioMetals* **2002**, *15*, 325.
(3) Braun, V.; Killmann, H. *Trends Biol. Sci.* **1999**, *24*, 104.
(4) Albrecht-Gary, A.-M.; Crumbliss, A. L. In *Metal Ions in Biological Systems*; Sigel, A., Sigel, H., Eds.; Marcel Dekker: New York, 1998; Vol. 35, p 239.
(5) Crumbliss, A. L. In *Handbook of Microbial Iron Chelates*; Winkelmann, G., Ed.; CRC Press: Boca Raton, FL, 1991; p 177.
(6) Matzanke, B. F.; Müller-Matzanke, G.; Raymond, K. N. In *Iron Carriers and Iron Proteins*; Loehr, T. M., Ed.; VCH Publishers: New York, 1989; Vol. 5, p 3.
(7) Neilands, J. B. *J. Biol. Chem.* **1995**, *270*, 26723.
(8) Raymond, K. N.; Telford, J. R. In *NATO ASI Series C, Mathematical and Physical Sciences*; Kessissoglous, D. P., Ed.; Kluwer Academic Publishers: Dordrecht, The Netherlands, 1995; Vol. 459, p 25.
(9) Winkelmann, G. *Handbook of Microbial Iron Chelates*; CRC Press: Boca Raton, FL, 1991.

10.1021/ic025647u CCC: $25.00
Published on Web 12/07/2002

at the cell surface by high-affinity siderophore receptors and enter the cell through outer membrane proteins in an energy-dependent process.[1,10−15] The iron-release mechanism, the final step of siderophore-mediated microbial iron transport, ultimately involves ligand exchange; hydrolysis of the siderophore ligand; and/or protonation of the iron−siderophore complex, which might be preceded by Fe(III) reduction.[2,4]

The desferrichromes, a class of structurally related fungal siderophores, are trihydroxamates and represent one of the very well studied siderophore systems.[9] All desferrichromes include a cyclic hexapeptide backbone containing a tripeptide sequence of N^{δ}-acyl-N^{δ}-hydroxy-L-ornithine, with the exception of tetraglycyl desferrichrome, a heptapeptide. The Fe(III)-chelating moieties in desferrichromes, hydroxamate groups, are located at the ends of three peptide arms that asymmetrically extend from the cyclic hexapeptide backbone (Figure 1).[16−20] Recent crystallographic data of ferrichrome bound to ferrichrome receptor and periplasmic binding protein show that the carbonyl oxygen donor atoms in the peptide backbone, as well as the oxygen atoms at the Fe(III) coordination shell, are involved in hydrogen-bonding interactions with the protein during the receptor and periplasmic binding protein recognition process.[17−23] This illustrates the critical role of both the backbone and the Fe(III) coordination shell in the receptor-recognition process. Over the years, various desferrichrome analogues have been synthesized in which the cyclic hexapeptide backbone is substituted by a series of scaffolds.[24−31] These synthetic

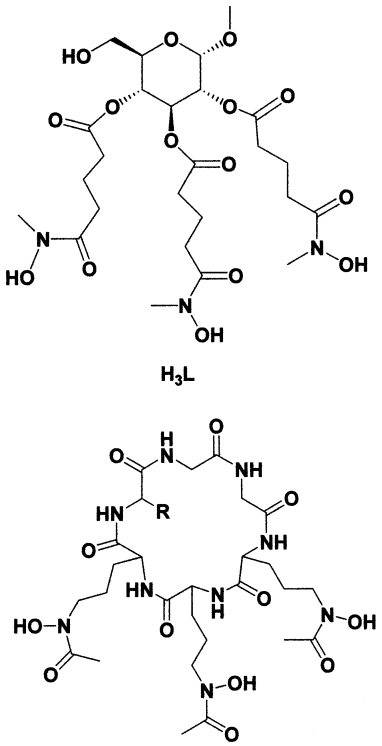

Figure 1. Desferrichrome and desferricrocin, naturally occurring exocyclic siderophores with hydroxamate functional groups, and a synthetic desferrichrome analogue with a saccharide backbone: 1-*O*-methyl-2,3,4-tris-*O*-[4-(*N*-hydroxy-*N*-methylcarbamoyl)-*n*-butyrate]-α-D-glucopyranoside (H_3L).

desferrichromeanalogues include triamine[24] and benzene[25] as the backbone. Such substitutions have been successful in maintaining a tripodal or exocyclic trihydroxamic acid structure for Fe(III) chelation, but in the process, the water solubility of these compounds is sacrificed, as well as the receptor-recognition capability of the backbone.

A series of synthetic analogues of enterobactin, an exocyclic triscatecholate siderophore produced by enteric bacteria, based on a carbohydrate backbone have recently been characterized with respect to their Fe(III) coordination chemistry.[32] These synthetic analogues have Fe(III) chelation capabilities comparable to that of the natural siderophore, enterobactin, and also show significant siderophore activities,[33] indicating favorable cell receptor recognition. This novel use of a carbohydrate as the scaffold for exocyclic tripodal siderophore analogues shows early promise in better elucidating siderophore-mediated iron transport, as well as providing significant synthetic flexibility in the design of these chelators. Here, we explore the possibilities of using a saccharide backbone to generate analogues of the desferrichrome family of hydroxamate siderophores.

A trihydroxamate analogue of desferrichrome (Figure 1) has been synthesized using a methyl α-D-glucopyranoside scaffold with three hydroxamic acid moieties per saccharide

(10) Letain, T. E.; Postie, K. *Mol. Microbiol.* **1997**, *24*, 271.
(11) Postle, K. *Mol. Microbiol* **1990**, *4*, 2019.
(12) Ecker, D. J.; Matzanke, B. F.; Raymond, K. N. *J. Bacteriol.* **1986**, *167*, 666.
(13) Armstrong, S. K.; McIntosh, M. A. *J. Biol. Chem.* **1995**, *270*, 2483.
(14) Newton, S. M. C.; Allen, J. S.; Cao, Z.; Qi, Z.; Jiang, X.; Sprencel, C.; Igo, J. D.; Foster, S. B.; Payne, M. A.; Klebba, P. E. *Proc. Natl. Acad. Sci.* **1997**, *94*, 4560.
(15) van der Helm, D. In *Metal Ions in Biological Systems*; Sigel, A., Sigel, H., Eds.; Marcel Dekker: New York, 1998; Vol. 35, p 355.
(16) Matzanke, B. F. In *Handbook of Microbial Iron Chelates*; Winkelmann, G., Ed.; CRC Press: Boca Raton, FL, 1991; p 15.
(17) Van der Helm, D.; Baker, J. R.; Eng-Wilmot, D. L.; Hossain, M. B.; Loghry, R. A. *J. Am. Chem. Soc.* **1980**, *102*, 4224.
(18) Zalkin, A.; Forrester, J. D.; Templeton, D. H. *Science* **1964**, *146*, 261.
(19) Zalkin, A.; Forrester, J. D.; Templeton, D. H. *J. Am. Chem. Soc.* **1966**, *88*, 1810.
(20) Norrestam, R.; Stensland, B.; Branden, C. I. *J. Mol. Biol.* **1975**, *99*, 501.
(21) Clarke, T. E.; Ku, S.-Y.; Dougan, D. R.; Vogel, H. J.; Tari, L. W. *Nat. Struct. Biol.* **2000**, *7*, 287.
(22) Ferguson, A. D.; Hofmann, E.; Coulton, J. W.; Diederichs, K.; Wolfram, W. *Science* **1998**, *282*, 2215.
(23) Locher, K. P.; Rees, B.; Koebnik, R.; Mitschler, A.; Moulinier, L.; Rosenbusch, J. P.; Moras, D. *Cell* **1998**, *95*, 771.
(24) Ng, C. Y.; Rodgers, S. J.; Raymond, K. N. *Inorg. Chem.* **1989**, *28*, 2062.
(25) Yoshida, I.; Murase, I.; Motekaitis, R. J.; Martell, A. E. *Can. J. Chem.* **1983**, *61*, 2740.
(26) Esteves, M. A.; Vaz, M. C. T.; Goncalves, M. L. S. S.; Farkas, E.; Santos, M. A. *J. Chem. Soc., Dalton Trans.* **1995**, 2565.
(27) Shanzer, A.; Libman, J. In *Metal Ions in Biological Systems*; Sigel, A., Sigel, H., Eds.; Marcel Dekker: New York, 1998; Vol. 35, p 329.
(28) Hara, Y.; Shen, L.; Tsubouchi, A.; Akiyama, M.; Umemoto, K. *Inorg. Chem.* **2000**, *39*, 5074.
(29) Hara, Y.; Akiyama, M. *J. Am. Chem. Soc.* **2001**, *123*, 7247.
(30) Tsubouchi, A.; Shen, L.; Hara, Y.; Akiyama, M. *New J. Chem.* **2001**, *25*, 275.
(31) Matssumoto, K.; Ozawa, T.; Jitsukawa, K.; Einaga, H.; Masuda, H. *Chem. Commun.* **2001**, 978.
(32) Dhungana, S.; Heggemann, S.; Heinisch, L.; Möllmann, U.; Boukhalfa, H.; Crumbliss, A. L. *Inorg. Chem.* **2001**, *40*, 7079.
(33) Heggemann, S.; Schnabelrauch, M.; Klemm, D.; Möllmann, U.; Reissbrodt, R.; Heinisch, L. *BioMetals* **2001**, *14*, 1.

unit: 1-*O*-methyl-2,3,4-tris-*O*-[4-(*N*-hydroxy-*N*-methylcarbamoyl)-*n*-butyrate]-α-D-glucopyranoside (H_3L).[34] This first example of a desferrichrome model with a carbohydrate backbone is a retrohydroxamate siderophore analogue (siderophore analogue in which the positions of the hydroxamate nitrogen and carbon are interchanged relative to their positions in the natural siderophore). Previous work on hydroxamate systems covalently linked to a saccharide unit are limited and include only monohydroxamates.[35] The saccharide scaffold allows for an asymmetrical distribution of the Fe(III)-binding hydroxamate arms and also increases the hydrophilicity of the molecule, unlike previously synthesized desferrichrome analogues. The presence of oxygen atoms in and around the saccharide ring gives the cyclic backbone the ability to act as a hydrogen-bond-acceptor during the cell receptor-recognition process. This structural property is comparable to the hydrogen-bond-accepting capacity of the carbonyl groups that are present on the natural desferrichrome backbone. Such synthetic analogues, therefore, are expected to be more complete models for desferrichrome and might be of significant interest as they can be used as penetration vectors for antibiotics or other biological applications involving Fe(III) uptake and metabolism. This article describes the aqueous solution characterization of the Fe(III)- and Fe(II)-chelating ability of H_3L.

Experimental Section

All solutions were prepared in deionized water. All pH measurements were made using a Corning 250 pH/ion meter equipped with an Orion ROSS pH electrode filled with 3.0 M NaCl solution. The pH's of all solutions were adjusted accordingly with NaOH or $HClO_4$. A stock solution of 2.0 M $NaClO_4$ was prepared from solid sodium perchlorate hydrate (Aldrich >99%) and allowed to pass through a Dowex 50 W-X8 strong acid cation-exchange column in H^+ form. The acid displaced from the column was titrated with standard NaOH solution to the phenolphthalein end point to obtain a standardized $NaClO_4$ solution. The 2.0 M $HClO_4$ stock solution was prepared from concentrated perchloric acid (Fisher 70%) and standardized by titration with standard NaOH solution to the phenolphthalein end point. Iron(III) perchlorate stock solution (0.1 M) was prepared from recrystallized iron(III) perchlorate (Aldrich), standardized spectrophotometrically in strong acid[36] and titrimetrically by reduction with Sn(II), and titrated with the primary standard potassium dichromate.[37] Carbonate-free NaOH was prepared by diluting Fisher 1 M NaOH with deionized water purged with Ar for 45 min and standardized by titration with standard 0.2000 M HCl (Fisher) to the phenolphthalein end point. A glass bulb electrode (Corning high performance) was used for the measurement of pH. The glass electrode was calibrated to read pH according to the classical method.[38]

The synthesis and characterization of 1-*O*-methyl-2,3,4-tris-*O*-[4-(*N*-hydroxy-*N*-methylcarbamoyl)-*n*-butyrate]-α-D-glucopyranoside (H_3L) are described elsewhere.[34] The tris(hydroxamate)iron(III) complex [$Fe^{III}L$] was formed by adding 1 equiv of $Fe^{3+}_{(aq)}$ to an aqueous solution of the ligand and slowly increasing the pH to 9 with constant stirring over the course of 30 min.

Methods. Potentiometric Measurements. Samples (10.00 mL) were placed in a double-walled titration cell maintained at 25.00 ± 0.05 °C by a circulating constant-temperature bath. Solutions were adjusted to $I = 0.10$ M by the addition of 2.0 M $NaClO_4$, and all solutions were purged with Ar prior to titration. A Titronic 96 standard buret was used for the titration; data were analyzed with the software SUPERQUAD.[39]

Spectrophotometric Measurements. UV−visible spectra were recorded using a Cary 100 spectrophotometer. All solutions were adjusted to $I = 0.10$ M by the addition of 2.0 M $NaClO_4$. The UV−visible spectra of the iron complexes as a function of pH were obtained from a single stock solution. The stock solution was divided into various batches, and each batch was used separately for the spectrophotometric titration. Titrations were carried out in both directions, from low pH to high pH and from high pH to low pH, using different batches of iron complexes. After each adjustment of pH, the solution was allowed to equilibrate for 10−15 min, after which an aliquot was taken and its visible spectrum was recorded. At low and high pH, the dilution due to the addition of concentrated acid and base, respectively, was corrected accordingly; data were analyzed using the software LETAGROP-SPEFO.[40] In spectrophotometric competition experiments with EDTA, 5.0-mL samples were allowed to equilibrate for 48 h at 25 °C. Typical solutions were 1×10^{-4} M in Fe(III) and the trihydroxamic acid ligand, with up to a 6-fold excess of EDTA (Aldrich). The protonation and Fe(III) formation constants for EDTA were taken from the critical compilation of Martell and Smith.[41]

Electrochemistry. The electrochemical behavior of the Fe^{III}−H_3L complex was studied in aqueous solution with 0.10 M $NaClO_4$ as the supporting electrolyte. Experiments were carried out using an EG&G Princeton Applied Research model 263 potentiostat. Voltammograms were recorded using PowerCV cyclic voltammetry software. All experiments were carried out under an Ar atmosphere at room temperature. The voltammograms were recorded at a scan rate of 100 mV/s with a HDME working electrode, Ag/AgCl (KCl saturated) reference electrode and platinum wire auxiliary electrode. Typical solutions were 1×10^{-3} M in Fe(III) and 1×10^{-2} M in ligand. The pH of the solution was adjusted using 1.0 M NaOH and 2.0 M $HClO_4$. Observed potentials referenced to Ag/AgCl (KCl saturated) were converted into NHE by adding 197 mV.

Results

Ligand Deprotonation Constants. The compound 1-*O*-methyl-2,3,4-tris-*O*-[4-(*N*-hydroxy-*N*-methylcarbamoyl)-*n*-butyrate]-α-D-glucopyranoside (H_3L) (Figure 1) is very soluble in water and, when dissolved in 0.10 M $NaClO_4$, gave a solution of pH 5.92. The ligand H_3L is a trihydroxamic acid, and the three deprotonation constants were determined by potentiometric titration. The potentiometric equilibrium curves for free H_3L and its Fe(III) complex are shown in Figure 2. The ligand deprotonation constants, K_{4-n} ($n = 1-3$), are defined by eqs 1 and 2 and are listed in Table 1 as pK_{4-n} [$-\log(K_{4-n})$], along with those of analogous

(34) Heggemann, S.; Möllmann, U.; Gebhardt, P.; Heinisch, L. *BioMetals*, in press.
(35) Ursic, S.; Zorc, B.; Pilepic, V.; Vikic-Topic, D. *Croat. Chem. Acta* **1993**, *65*, 851.
(36) Bastian, R.; Weberling, R.; Palilla, F. *Anal. Chem.* **1956**, *28*, 459.
(37) Vogel, A. I. *Quantitative Inorganic Analysis Including Elementary Instrumental Analysis*, 3rd ed.; Longmans, Green and Co., Ltd.: London, 1968.
(38) Martell, A. E.; Motekaitis, R. J. *Determination and Use of Stability Constants*, 2nd ed.; VCH Publishers: New York, 1992.
(39) Gans, P.; Sabatini, A.; Vacca, A. *J. Chem. Soc., Dalton Trans.* **1985**, 1195.
(40) Sillen, L. G.; Warsquist, B. *Ark. Kemi* **1968**, *31*, 377.
(41) Martell, A. E.; Smith, R. M. *Critical Stability Constants*; Plenum Press: New York, 1974; Vol. 1.

Table 1. Ligand pK_a Values for H_3L and Relevant Natural and Synthetic Siderophores

	pK_{4-n}[a]				
n	H_3L[b]	desferrichrome[c]	desferricrocin[d]	desferrioxamine B[c]	TRENDROX[e]
3	8.67 ± 0.03	8.11	8.14	8.39	8.58
2	9.31 ± 0.01	9.00	9.01	9.03	9.33
1	9.94 ± 0.01	9.83	9.92	9.70	10.30

[a] Defined by eq 2. [b] Conditions: $T = 298$ K and $\mu = 0.10$ M $NaClO_4$. [c] References 45 and 48. [d] Reference 46. [e] Reference 24.

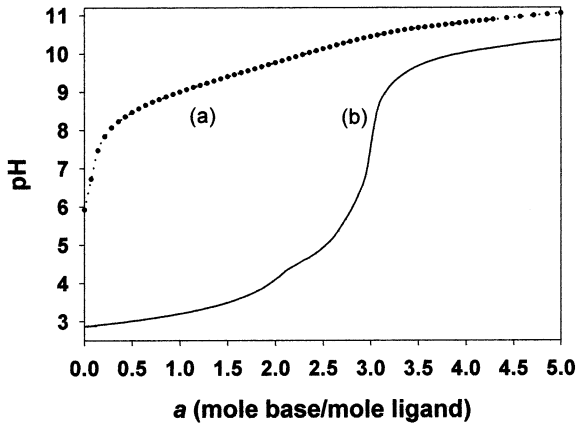

Figure 2. Potentiometric titration curves: (a) 5.9×10^{-4} M H_3L; (b) $H_3L/Fe^{3+} = 1:1$, 5.9×10^{-4} M. Conditions: $T = 298$ K and $\mu = 0.10$ M $NaClO_4$.

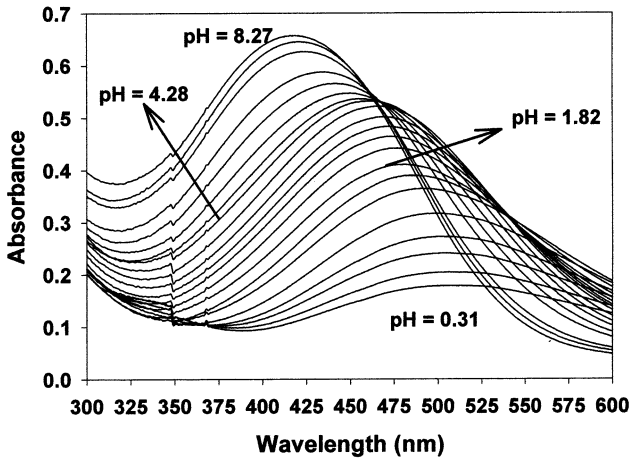

Figure 3. Spectrophotometric titration: UV−visible spectra of $Fe^{III}-H_3L$ as a function of pH from pH 0.31 to 8.27. Conditions: $H_3L/Fe^{3+} = 1:1$, 2.0×10^{-4} M; $T = 298$ K; and $\mu = 0.10$ M $NaClO_4$.

trihydroxamic acids.

$$H_nL^{-3+n} \overset{K_{4-n}}{\rightleftharpoons} H_{n-1}L^{-4+n} + H^+ \quad (1)$$

$$K_{4-n} = \frac{[H_{n-1}L^{-4+n}][H^+]}{[H_nL^{-3+n}]} \quad (2)$$

The acid dissociation constants for H_3L fall in the normal range (p$K_a = 8-10$) for hydroxamic acids[42−44] and are in good agreement with the acid dissociation constants for analogous trihydroxamic acids (Table 1).[24,45,46] The pK_a's for H_3L are slightly higher than those of the natural trihydroxamate siderophores (desferrichrome, desferricrocin, and desferrioxamine B)[45,46] and are comparable to those of the synthetic retrohydroxamate TRENDROX.[24] The deprotonation constants are evenly separated from each other and display only slightly greater (0.63 and 0.64 log unit) than the statistical separation of 0.48 log unit. This suggests that there is no significant intramolecular interaction between the three hydroxamate groups.

Fe(III) Complex Formation and Protonation Constants. (a) General Considerations. The potentiometric titration curve for H_3L in the presence of an equivalent concentration of Fe(III) (Figure 2) shows a slight inflection at $a = 2$ and a clear inflection point at $a = 3$. The inflection at 2 mol of base/mol of H_3L ($a = 2$) occurs in the pH range 4.3−4.7, where the solution is deep red with $\lambda_{max} = 465$ nm ($\epsilon = 2100$ M^{-1} cm^{-1}). The absorbance band at 465 nm (Figure 3) is assigned to a ligand-to-metal charge transfer (LMCT) for the iron(III)−dihydroxamate complex [$Fe^{III}HL(H_2O)_2^+$], and the release of two protons ($a = 2$) during the potentiometric titration is consistent with the formation of a bis(hydroxamate) complex. These spectrophotometric and potentiometric titration observations are consistent with those corresponding to the bis(hydroxamate) complexes of monohydroxamic acids with Fe(III) and bis(hydroxamate) complexes of other trihydroxamic acids with Fe(III).[4,5] The inflection point at $a = 3$ (Figure 2) indicates a release of three protons during the course of the titration and occurs at pH = 7. At this point, the solution becomes reddish orange with $\lambda_{max} = 416$ nm ($\epsilon = 2900$ M^{-1} cm^{-1}) (Figure 3). This transition is assigned to a ligand-to-metal charge transfer (LMCT) for the tris(hydroxamate)−iron(III) complex, as these complexes give a characteristic LMCT band at 415−425 nm. These parameters and qualitative aspects of the UV−visible spectra are very similar to those corresponding to the tris(hydroxamate) complex of monohydroxamic acids with Fe(III), such as acetohydroxamic acid and other tris(bidentate) model compounds that coordinate to Fe(III) through six oxygen atoms on the hydroxamate moieties.[4,5] Both the spectrophotometric and the potentiometric titrations indicate that, at pH > 7, a single species is formed, accompanied by the displacement of three protons. During the course of both spectrophotometic and potentiometric titrations, two distinct Fe(III) complexes were observed over two pH ranges, and they can be identified as the bis(hydroxamate)−iron(III) complex, $Fe^{III}HL(H_2O)_2^+$, and the tris(hydroxamate)−iron(III) complex, $Fe^{III}L$.

(42) Brink, C. P.; Crumbliss, A. L. *J. Org. Chem.* **1982**, *47*, 1171.
(43) Brink, C. P.; Fish, L. L.; Crumbliss, A. L. *J. Org. Chem.* **1985**, *50*, 2277.
(44) Monzyk, B.; Crumbliss, A. L. *J. Org. Chem.* **1980**, *45*, 4670.
(45) Anderegg, G.; L'Eplattenier, F.; Schwarzenbach, G. *Helv. Chim. Acta* **1963**, *46*, 1409.
(46) Wong, G. B.; Kappel, M. J.; Raymond, K. N.; Matzanke, B.; Winkelmann, G. *J. Am. Chem. Soc.* **1983**, *105*, 810.

The spectrophotometric titration was carried out separately in both directions, from low pH to high pH and from high pH to low pH, with identical results. A spectral profile for the titration going from low pH to high pH is shown in Figure 3. Above pH = 7, there was no significant change in the LMCT bands, indicating complete formation of the tris complex $Fe^{III}L$. However, at a much higher pH, 9.5, the complex irreversibly hydrolyzes with loss of the characteristic LMCT bands.

(b) $Fe^{III}L$ Complex Equilibria. The potentiometric titration curve for H_3L in the presence of Fe(III) exhibits a large jump at $a = 3$, as expected for the three protons of the hydroxamate groups (Figure 2). This steep inflection at $a = 3$ indicates tight Fe(III) binding. The titration curve also has a small inflection at $a = 2$ in the pH range 4.2−4.7. The pH values corresponding to $a = 2.5$ and $a = 1.5$ represent the first and second protonation constants of $Fe^{III}L$, respectively.

Spectrophotometric titration of the $Fe^{III}-H_3L$ complex allowed us to determine the complex protonation constants by observing the changes in the intense LMCT band of the metal complex. The UV−visible spectra of $Fe^{III}-H_3L$ as a function of pH are shown in Figure 3. As discussed earlier, the pH-dependent spectral profile clearly indicates the presence of the tris(hydroxamate)−iron(III) complex above pH = 8. As the pH of the $Fe^{III}L$ complex is lowered, λ_{max} shifts to longer wavelength, 465 nm. This new λ_{max} also corresponds to the first isosbestic point, which clearly extends over the pH range of 4−8. This isosbestic point indicates that, over this pH range, a simple equilibrium exists between two different metal complexes. This equilibrium results from the protonation and subsequent dissociation of one of the three hydroxamate groups in $Fe^{III}L$ to give the bishydroxamate complex, $Fe^{III}HL(H_2O)_2^{+}$, consistent with other monohydroxamic acid Fe(III) equilibria previously reported.[4,5] In the potentiometric titration, this equilibrium has equal concentrations of the two species at $a = 2.5$, and the corresponding pH value of ca. 4.8 can be approximated as the logarithm of the first protonation constant of the $Fe^{III}L$ complex. The corresponding protonation equilibrium is indicated by eq 3, and the protonation constant $K_{Fe^{III}HL}$ is defined by eq 4.

$$Fe^{III}L + H^{+} \rightleftharpoons Fe^{III}HL(H_2O)_2^{+} \quad (3)$$

$$K_{Fe^{III}HL} = \frac{[Fe^{III}HL(H_2O)_2^{+}]}{[Fe^{III}L][H^{+}]} \quad (4)$$

As the pH is lowered further, the absorbance of $Fe^{III}HL(H_2O)_2^{+}$ gradually decreases, and λ_{max} shifts to longer wavelength, 510 nm ($\epsilon = 950\ M^{-1}\ cm^{-1}$), typical of a mono(hydroxamate)−iron(III) complex. Protonation of the bis(hydroxamate)−iron(III) complex, $Fe^{III}HL(H_2O)_2^{+}$, involves protonation of one of the two hydroxamate groups coordinated to Fe(III) and its subsequent dissociation to give a mono(hydroxamate)−iron(III) complex, $Fe^{III}H_2L(H_2O)_4^{2+}$. The absorbance due to LMCT bands of the mono(hydroxamate)−iron(III) complex, $Fe^{III}H_2L(H_2O)_4^{2+}$, starts to fade with further decreases in pH while maintaining λ_{max} at 510 nm. Such a gradual decrease in the LMCT bands at a stationary λ_{max} of 510 nm indicates that the concentration of $Fe^{III}H_2L(H_2O)_4^{2+}$ is being depleted as the pH is lowered below pH = 1. This suggests that, at low pH, there is a further protonation of the mono(hydroxamate)−iron(III) complex, with subsequent dissociation to a free triprotonated ligand, H_3L, and hexaaquo-iron(III) species, $Fe^{III}(H_2O)_6^{3+}$. This is consistent with the gradual decrease in the LMCT band with a fixed λ_{max} of 510 nm. During the course of the experiment, even at a pH as low as 0.3, the LMCT band was observed. This suggests that the mono(hydroxamate)−iron(III) complex is quite stable even at low pH.

Table 2. Protonation Constants for FeL and Ferrioxamine B

	FeL[a]		ferrioxamine B	
	Fe(III)[b]	Fe(II)[c]	Fe(III)[b]	Fe(II)[c]
$\log K_{FeHL}$	4.69 ± 0.05 4.2 ± 0.2[f]	6.6 ± 0.1	0.94[d]	3.2[e]
$\log K_{FeH_2L}$	2.41 ± 0.10	5.1 ± 0.2	−	−
$\log K_{FeH_3L}$	0.61 ± 0.22	4.0 ± 0.2	−	−

[a] Conditions: $T = 298$ K and $\mu = 0.10$ M $NaClO_4$. [b] As defined by eqs 4, 6, and 8. [c] As defined by eqs 19 and 20. [d] Reference 53. [e] Reference 2. [f] Calculated from electrochemical data in Figure 6 using eq 21.

The protonation and subsequent dissociation model for the second and third protonation processes are represented by eqs 5 and 7, and the corresponding protonation constants are defined by eqs 6 and 8, respectively.

$$Fe^{III}HL(H_2O)_2^{+} + H^{+} \rightleftharpoons Fe^{III}H_2L(H_2O)_4^{2+} \quad (5)$$

$$K_{Fe^{III}H_2L} = \frac{[Fe^{III}H_2L(H_2O)_4^{2+}]}{[Fe^{III}HL(H_2O)_2^{+}][H^{+}]} \quad (6)$$

$$Fe^{III}H_2L(H_2O)_4^{2+} + H^{+} \rightleftharpoons Fe^{III}(H_2O)_6^{3+} + H_3L \quad (7)$$

$$K_{Fe^{III}H_3L} = \frac{[Fe^{III}(H_2O)_6^{3+}][H_3L]}{[Fe^{III}H_2L(H_2O)_4^{2+}][H^{+}]} \quad (8)$$

The protonation constants for $Fe^{III}L$ were calculated by refining the entire spectrophotometric data set using the software LETAGROP-SPEFO[40] to fit the above-described model. This model fits the data well, as indicated by the small standard deviations for the protonation constants tabulated in Table 2. The logarithm of the first protonation constant (eqs 3 and 4), $\log K_{Fe^{III}HL}$, was spectrophotometrically determined to be 4.69. This value is consistent with the isosbestic point at 465 nm in the pH range 4.2−4.7 during the spectrophotometric titration (Figure 3). The $\log K_{Fe^{III}HL}$ value is also consistent with the potentiometric data, where the pH value corresponding to $a = 2.5$ is ca. 4.8 (Figure 2). Unlike the first protonation step, there is no distinct qualitative evidence for the second and third protonation steps during both potentiometric and spectrophotometric titrations; however, the protonation constants determined fall within the spectral profile determined by the spectrophotometic titration. This agreement, as well as the very good fit of the above model to the data, supports the validity of the values

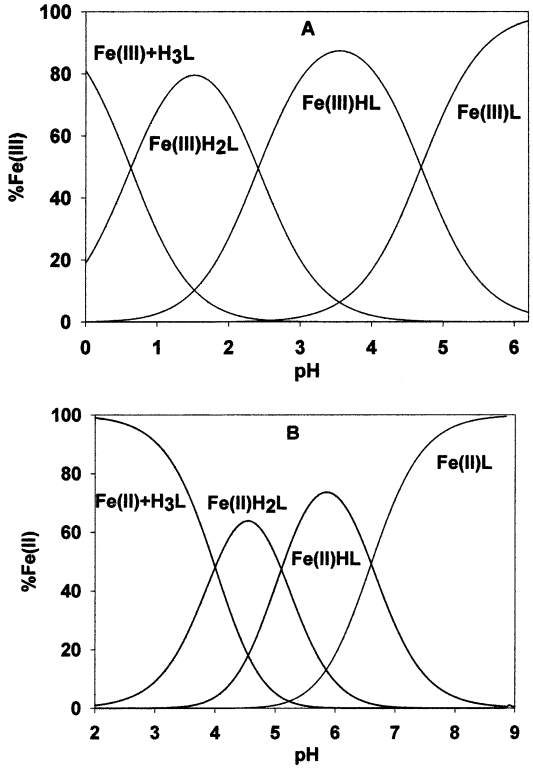

Figure 4. Calculated species distribution for (A) Fe(III) and (B) Fe(II) complexes of H_3L. Metal-containing species are normalized to the total concentration of iron. Coordinated water molecules omitted for clarity. Conditions: $H_3L/Fe^{3+} = 1:1$, $T = 298$ K, and $\mu = 0.10$ M $NaClO_4$.

determined for these protonation constants. In addition, the above-determined protonation constants are in good agreement with those reported for certain tripodal synthetic analogues of desferrichrome.[47]

(c) Overall Complex Stability and Species Distribution. The protonation constants that were determined for $Fe^{III}L$ were used to generate a species distribution curve (Figure 4A). The speciation diagram for the $Fe^{III}-H_3L$ system clearly shows that all three iron(III)−hydroxamate species, $Fe^{III}L$, $Fe^{III}HL(H_2O)_2^{+}$, and $Fe^{III}H_2L(H_2O)_4^{2+}$, are present as significantly abundant species over a distinct pH range. At pH = 1.5, $Fe^{III}H_2L(H_2O)_4^{2+}$ is the major species; at pH = 3.6, $Fe^{III}HL(H_2O)_2^{+}$ is the predominate species; and above pH = 6, $Fe^{III}L$ becomes the only species present.

The overall stability constant, log β_{110}^{III} (defined by eqs 9 and 10), for $Fe^{III}L$ was calculated using the software LETAGROP-SPEFO[40] and data from the spectrophotometric titration (Table 3). The stability constant for $Fe^{III}L$ is higher than those of ferrichrome and the other natural hydroxamate siderophores listed in Table 3.[24,45,46,48]

$$Fe_{(aq)}^{3+} + L^{3-} \rightleftharpoons FeL \tag{9}$$

$$\beta_{110}^{III} = \frac{[FeL]}{[Fe_{(aq)}^{3+}][L^{3-}]} \tag{10}$$

(47) Motekaitis, R. J.; Sun, Y.; Martell, A. E. *Inorg. Chem.* **1991**, *30*, 1554.
(48) Schwarzenbach, G.; Schwarzenbach, K. *Helv. Chim. Acta* **1963**, *46*, 1390.

Table 3. Fe−Siderophore Complex Thermodynamic Parameters

ligand	log β_{110}[a] Fe(III)	log β_{110}[a] Fe(II)	pFe[b]	$E_{1/2}$ vs NHE (mV)	ref
H_3L[c]	31.86 ± 0.11	12.1	27.1	−436	this work
desferrichrome	29.07	9.9	25.2	−400	45, 54
desferricrocin	30.4	11.6	26.5	−412	46
desferrioxamine B	30.60	10.3	26.6	−468	48, 52, 55, 56
TRENDROX	32.9	−	27.8		24

[a] Defined as $\beta_{110} = [FeL]/[Fe][L]$ for Fe + L ⇌ FeL (charges omitted for clarity). [b] $-\log[Fe^{3+}]$ at $[Fe(III)]_{tot} = 10^{-6}$ M, $[ligand]_{tot} = 10^{-5}$ M, and pH = 7.4. [c] Conditions: $T = 298$ K and $\mu = 0.10$ M $NaClO_4$.

The log β_{110}^{III} for $Fe^{III}L$ was also determined by spectrophotometric competition experiments with EDTA at pH 8.91. The competition equilibrium is described by eqs 11 and 12.

$$Fe^{III}L + EDTA \overset{K}{\rightleftharpoons} Fe^{III}EDTA + L \tag{11}$$

$$K = \frac{[Fe^{III}EDTA][L]}{[Fe^{III}L][EDTA]} = \frac{\beta_{110}^{FeEDTA}}{\beta_{110}^{Fe(III)L}} \tag{12}$$

The molecular charges and water molecules involved in the equilibrium are omitted for clarity. The concentrations of $Fe^{III}L$ were calculated from the absorbance at 416 nm, where $Fe^{III}L$ is the only light-absorbing species. The concentrations of other species in eq 12 were calculated from mass balance equations using the experimental pH values

$$[Fe]_{tot} = \alpha_{Fe^{III}L}[Fe^{III}L] + \alpha_{Fe^{III}EDTA}[Fe^{III}EDTA] \tag{13}$$

$$[L]_{tot} = \alpha_{Fe^{III}L}[Fe^{III}L] + \alpha_{L}[L] \tag{14}$$

$$[EDTA]_{tot} = \alpha_{Fe^{III}EDTA}[Fe^{III}EDTA] + \alpha_{EDTA}[EDTA] \tag{15}$$

where α is the usual Ringbom's coefficient.[49] The stability constant, log β_{110}^{III}, for $Fe^{III}L$ was calculated using the relationship defined by eq 12 and found to be 31.1, in excellent agreement with the value determined from the spectrophotometric titration.

To compare the Fe(III)-chelating properties of H_3L with other Fe(III) chelators at physiological conditions, the pFe values were calculated ($-\log[Fe^{3+}]$ at pH = 7.4 with a total ligand concentration, $[L]_{tot}$, of 10^{-5} M and total Fe(III) concentration of 10^{-6} M).[50] The concentration of free Fe(III) ion in solution can be expressed by eq 16

$$[Fe^{III}] = \frac{[FeL]_{tot}}{\beta_{110}^{III}[(L)_{tot} - (FeL)_{tot}]} = \frac{\alpha_L}{9(\alpha_{Fe^{III}L})\beta_{110}^{III}} \tag{16}$$

where β_{110}^{III} represents the overall stability constant for Fe(III) and α_L and $\alpha_{Fe^{III}L}$ are the usual Ringbom's coefficients[49] for the ligand and the iron−ligand complex, respectively. The pFe for H_3L was calculated to be 27.1, which is

(49) Ringbom, A. *Complexation in Analytical Chemistry: A Guide for the Critical Selection of Analytical Methods Based on Complexation Reactions*; Interscience Publishers: New York, 1963.
(50) Raymond, K. N.; Müller, G.; Matzanke, B. F. In *Topics in Current Chemistry*; Boschke, F. L., Ed.; Springer-Verlag: Berlin, 1984; Vol. 123, p 49.

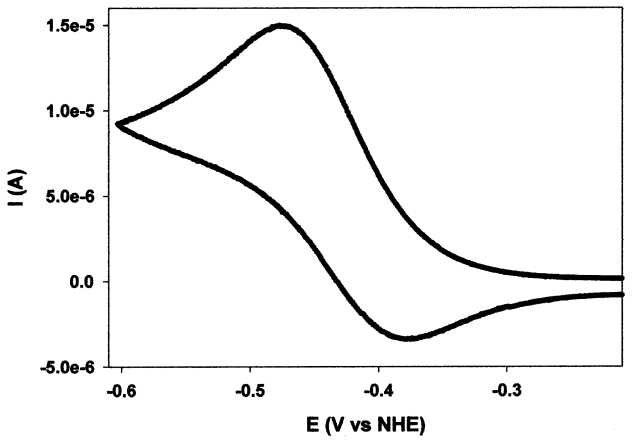

Figure 5. Cyclic voltammogram of $Fe^{III}L$. Conditions: [Fe] = 1×10^{-3} M, [H_3L] = 1×10^{-2} M, pH = 9.5, HDME working electrode, scan rate = 100 mV/s, T = 298 K, and μ = 0.10 M ($NaClO_4$). $E_{1/2}$ = −436 mV with a peak separation of 90 mV.

comparable or greater than the values calculated for desferrichrome and desferrichrome analogues (Table 3), and is significantly higher than that of transferrin, 23.6.[51]

(d) Electrochemistry and Fe(II) Chelation. Reversible electrochemistry is illustrated by the cyclic voltammogram for $Fe^{III}L$ (Figure 5) corresponding to an Fe(III)/Fe(II) couple with a half-wave potential ($E_{1/2}$) of −436 mV vs NHE at pH = 9.5. The negative reduction potential for the Fe(III)/Fe(II) couple indicates that H_3L has great selectivity for Fe(III) over Fe(II). This selectivity is directly related to the stability constants for the Fe(III) and Fe(II) complexes of H_3L and is described by eq 17

$$E_{aquo} - E^{\circ}_{complex} = 59.15 \log(\beta^{III}_{110}/\beta^{II}_{110}) \qquad (17)$$

where β^{III}_{110} and β^{II}_{110} represent the overall stability constant for the Fe(III) and Fe(II) oxidation states, respectively. The $Fe^{II}L^-$ stability constant for H_3L was calculated (Table 3) and found to be in good agreement with values reported for desferrichrome and desferrichrome analogues. An E_{aquo} value of +732 mV was used for the above calculation to be consistent with our previous work.[52]

The pH dependence of the cyclic voltammogram shows a gradual positive shift in the reduction potential for the Fe(III)/Fe(II) couple as the pH is lowered. The cyclic voltammogram remains reversible until pH = 7. As the pH is lowered below pH = 7, the voltammogram becomes quasi-reversible and finally irreversible. The $E_{1/2}$ values for such irreversible pH-dependent voltammograms were calculated assuming a peak-to-peak separation of 90 mV, as observed in the reversible case at pH = 9.5. The observed $E_{1/2}$ is strongly pH-dependent (Figure 6) and is attributed to the protonation and ultimate dissociation of the hydroxamate groups in the Fe(II) complex after the reduction of the Fe(III) complex as represented by eqs 18−20, along with the protonation of $Fe^{III}L$ complex (eq 3) over the

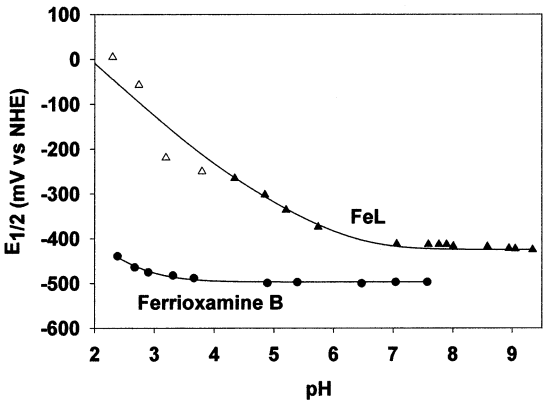

Figure 6. $Fe^{III}L$ reduction potential ($E_{1/2}$) as a function of pH (upper curve, triangles). Conditions: [Fe] = 1×10^{-3} M, [H_3L] = 1×10^{-2} M, HDME working electrode, scan rate = 100 mV/s, T = 298 K, and μ = 0.10 M ($NaClO_4$). The solid triangles represent data points used in the nonlinear regression analysis. The solid line represents a plot of eq 21, where E°_{Fe} = +732 mV; $\beta^{III}_{110} = 10^{31.86}$; $\beta^{II}_{110} = 10^{12.1}$; $K_{Fe^{III}HL} = 10^{4.69}$; and $K_{Fe^{II}HL}$, $K_{Fe^{II}H_2L}$, and $K_{Fe^{II}H_3L}$ were determined by non linear least-squares analysis to be $10^{6.6}$, $10^{5.1}$, and $10^{4.0}$, respectively. The ferrioxamine B data (lower curve) are from ref 2; the solid line represents a plot of the equation $E_f = E^{\circ}_{Fe} - 59.15 \log\{\beta^{III}_{110}/\beta^{II}_{110}\} + 59.15 \log(1 + K_{Fe^{II}HL}[H^+])$, where E°_{Fe} = +732 mV, $\beta^{III}_{110} = 10^{30.60}$, $\beta^{II}_{110} = 10^{10.3}$, and $K_{Fe^{II}HL}$ was determined from nonlinear least-squares analysis to be $10^{3.2}$.

experimental pH range.

$$Fe^{III}L + e^- \rightleftharpoons {}^-Fe^{II}L^- \qquad (18)$$

$$Fe^{II}H_{n-1}L^{-2+n} + H^+ \overset{K_{Fe^{II}H_nL}}{\rightleftharpoons} Fe^{II}H_nL(H_2O)_{2n}{}^{-1+n} \qquad (19)$$

$$K_{Fe^{II}H_nL} = \frac{[Fe^{II}H_nL(H_2O)_{2n}{}^{-1+n}]}{[Fe^{II}H_{n-1}L^{-2+n}][H^+]} \qquad (20)$$

The pH dependence of the reduction potential profile in Figure 6 corresponds to four distinct single protonation reactions; three protonation reactions for three different Fe(II) complexes and a protonation of the $Fe^{III}L$ complex. For such a system, the observed formal reduction potential should vary as

$$E_f = E^{\circ}_{Fe} - 59.15 \log\left(\frac{\beta^{III}_{110}}{\beta^{II}_{110}}\right) + 59.15 \log(1 + K_{Fe^{III}HL}[H^+] + K_{Fe^{III}HL}K_{Fe^{II}H_2L}[H^+]^2 + K_{Fe^{III}HL}K_{Fe^{II}H_2L}K_{Fe^{II}H_3L}[H^+]^3) - 59.15 \log(1 + K_{Fe^{III}HL}[H^+]) \qquad (21)$$

where E°_{Fe} is the standard reduction potential of the Fe(III)/Fe(II) aquo couple; β^{III}_{110} and β^{II}_{110} are the overall stability constants for the Fe(III) and Fe(II) hexacoordinated complexes, respectively; $K_{Fe^{II}H_nL}$ represents the stepwise protonation constants of the Fe(II) complex (eqs 19 and 20); and $K_{Fe^{III}HL}$ is the first protonation constant of the Fe(III) complex (eqs 3 and 4). A nonlinear least-squares refinement of the data (Figure 6) using eq 21 with a fixed $K_{Fe^{III}HL}$ value of $10^{4.69}$ obtained from the spectrophotometric titration gave the Fe(II) complex protonation constants listed in Table 2. These constants were used to generate an $Fe^{II}-H_3L$ species distribution curve (Figure 4B) that clearly shows three

(51) Harris, W. R.; Carrano, C. J.; Cooper, S. R.; Sofen, S. R.; Avdeef, A.; McArdle, J. V.; Raymond, K. N. *J. Am. Chem. Soc.* **1979**, *101*, 6097.
(52) Spasojevic, I.; Armstrong, S. K.; Brickman, T. J.; Crumbliss, A. L. *Inorg. Chem.* **1999**, *38*, 449.

iron(II)−hydroxamate species, $Fe^{II}L^-$, $Fe^{II}HL(H_2O)_2$, and $Fe^{II}H_2L(H_2O)_4^+$, present as major species over three distinct pH ranges. At pH = 4.6 and 5.8, $Fe^{II}H_2L(H_2O)_4^+$ and $Fe^{II}HL(H_2O)_2$, respectively, are the predominate species, and above pH = 8.0, $Fe^{II}L^-$ becomes the only species present. The doubly protonated Fe(II) complex species, $Fe^{II}H_2L(H_2O)_4^+$, is only present at 65% abundance at its maximum at pH = 4.6. Below pH = 3.9, most of the $Fe^{II}-H_3L$ complex is dissociated to give $Fe^{II}(H_2O)_6^{2+}$ and free H_3L.

When the data presented in Figure 6 are analyzed using eq 21 and treating all of the protonation constants for $Fe^{III}L$ and $Fe^{II}L^-$ as variables, the values obtained for $K_{Fe^{II}H_nL}$ are virtually identical to those listed in Table 2, and the computed value for $K_{Fe^{III}HL}$ is $10^{4.2}$. This is in excellent agreement with the value determined by spectrophotometric titration (Table 2) and supports the validity of the model used for the pH-dependent electrochemical data analysis.

Discussion

The high overall stability of the $Fe^{III}L$ complex, compared to that of other trihydroxamic acid systems (Table 3), makes H_3L a very attractive model for desferrichrome. The proton-dependent equilibrium studies indicate three well-separated protonation steps for $Fe^{III}L$, and the protonation constants are significantly higher than those seen for other natural trihydroxamate systems, the desferrichromes and desferrioxamine B.[45,53] However, these protonation constants are similar to those determined for certain tipodal synthetic analogues of desferrichrome with both hydroxamate and retrohydroxamate as iron-binding moieties.[47] These protonation constants along with the ligand protonation constants influence the species distribution at various pH values (Figure 4) and directly reflect the relative chelating ability of the ligand under specific conditions. A more direct indication of this effectiveness is achieved by comparing the pFe values (Table 3). The pFe of H_3L is one of the highest among the trihydroxamate systems, both natural and synthetic, despite significantly higher $Fe^{III}L$ protonation constants. This is not surprising because, at pH = 7.4, where pFe is calculated, $Fe^{III}L$ is the predominant species (Figure 4). The high pFe of H_3L indicates that it is a very effective Fe(III)-chelating agent at physiological pH and, for example, is thermodynamically capable of removing Fe(III) from transferrin.

The species distribution curves (Figure 4) provide insight into a possible mechanism for iron release from the complex. Figure 4A indicates that, above pH = 6, $Fe^{III}L$ is the only species present in an Fe(III) system; however, upon reduction of $Fe^{III}L$ to $Fe^{II}L^-$, more than one Fe^{II} species are present (Figure 4B), even at the physiological pH of 7.4. This phenomenon is a result of the $Fe^{II}L^-$ protonation constants being consistently greater than the $Fe^{III}L$ protonation constants by 2 orders of magnitude (Table 2). Here, we see that an Fe(III/II) reduction process not only decreases the thermodynamic stability of the complex ($\beta^{III}_{110} = 10^{31.86}$, $\beta^{II}_{110} = 10^{12.1}$) and makes the complex more labile with respect to ligand exchange, but in addition makes it more susceptible to protonation.

A pH-dependent electrochemical study for ferrioxamine B[2] demonstrates that $E_{1/2}$ for ferrioxamine B is less sensitive to pH changes than $E_{1/2}$ for $Fe^{III}L$ (Figure 6). This suggests that ferrioxamine B and $Fe^{III}L$ behave similarly with respect to redox-dependent protonation reactions. $Fe^{III}L$ has greater stability (higher β^{III}_{110} and pFe) than ferrioxamine B, but because of higher Fe(II) protonation constants, its $E_{1/2}$ is more pH-sensitive, making a redox process for delivery of iron more facile compared to that of ferrioxamine B. Such an observation illustrates that the iron release mechanism in siderophore-mediated iron transport could be composed of two complementary processes involving reduction of the iron(III)−siderophore complex to an Fe(II) complex and its subsequent protonation. Both $Fe^{III}L$ and ferrioxamine B demonstrate that protonation of the Fe(II) complex can be achieved more easily than protonation of the Fe(III) complex. A reduction of the Fe(III) complex to an Fe(II) complex and a subsequent protonation of the reduced Fe(II) complex drastically changes the pH-dependent speciation profile (Figure 4) and can provide a pathway for overcoming the very high thermodynamic stability of iron(III)−siderophore complexes. Thus reduction results in the relatively facile dissociation of hydroxamate chelating groups to release the siderophore bound iron.

The biological activity of H_3L was examined by bioassays involving wild-type strains and iron transport mutants of mycobacteria and of Gram-negative bacteria. These studies indicated positive growth-promotion (siderophore) activity for H_3L. In general, H_3L displayed good growth-promotion activity for the selected Gram-negative bacteria, as well as activity for the wild-type and mutant strains of the mycobacteria. The details are reported separately.[34] Such positive growth promotion indicates that H_3L has features for favorable cell receptor recognition and thus is a good siderophore analogue, biologically as well as chemically.

The use of a saccharide as the ligand backbone has been shown to have a few distinct advantages. The presence of the saccharide ring significantly enhances the solubility of the ligand regardless of pH, a property lacking in other synthetic ferrichrome analogues, while maintaining a high degree of Fe(III) binding stability. The hydrogen-bond-accepting ability of oxygen atoms in and around the saccharide appears to provide the cyclic backbone with favorable cell receptor recognition. The biological activity displayed by H_3L over a large range of bacterial strains[34] certainly supports this hypothesis of receptor recognition. Finally, the large size of the saccharide ring appears to provide a very good backbone for the optimal encapsulation of the Fe(III) ion by the hydroxamate groups, as illustrated by the high overall stability of the $Fe^{III}-H_3L$ complex.

(53) Evers, A.; Hancock, R. D.; Martell, A. E.; Motekaitis, R. J. *Inorg. Chem.* **1989**, *28*, 2189.
(54) Wawrousek, E. F.; McArdle, J. V. *J. Inorg. Biochem.* **1982**, *17*, 169.
(55) Bickel, H.; Hall, G. E.; Keller-Schierlein, W.; Prelog, V.; Vischer, E.; Wettstein, A. *Helv. Chim. Acta* **1960**, *43*, 2129.
(56) Cooper, S. R.; McArdle, J. V.; Raymond, K. N. *Proc. Natl. Acad. Sci. U.S.A.* **1978**, *75* 3551.

Summary and Conclusions

The Fe(III) coordination chemistry of a new ferrichrome analogue, 1-*O*-methyl-2,3,4-tris-*O*-[4-(*N*-hydroxy-*N*-methylcarbamoyl)-*n*-butyrate]-α-D-glucopyranoside (H_3L), with a chiral saccharide backbone in aqueous solution was explored. The thermodynamic and spectroscopic properties of the Fe(III) complexes closely parallel those of iron-[ferrichrome], Fe(III) complexes of the ferrichrome family of siderophores, and other ferrichrome analogues. The Fe(III) binding affinity of H_3L is equivalent to or better than that reported for the ferrichromes and ferrichrome models. The very high pFe of H_3L suggests that it is an effective chelating agent at physiological conditions and, from a thermodynamic standpoint, could possibly be used to remove Fe(III) from transferrin. These thermodynamic and spectroscopic properties, along with the extensive hydrogen-bonding capability of the saccharide backbone, make such ferrichrome analogues very attractive systems for investigation as substrates for cell receptor proteins that recognize Fe(III) complexes of the ferrichromes. A comparative analysis of the $Fe^{III}L$ and $Fe^{II}L^-$ stabilities and protonation constants illustrates that one of the iron-release mechanisms in siderophore-mediated iron transport is likely the reduction of iron(III)−siderophore followed by protonation of iron(II)−siderophore and subsequent release of iron.

Acknowledgment. We (S.D. and A.L.C.) thank the National Science Foundation (CHE-0079066) for financial support.

IC025647U